Correlation Functions in Non-Newtonian Couette Flow

A Group Theory and Molecular Dynamics Approach

M. W. Evans† and D. M. Heyes*
Department of Chemistry, Royal Holloway and Bedford New College, University of London, Egham, Surrey TW20 0EX

We develop *new* aspects of the statistical mechanics of non-Newtonian shear flow. The phenomena of non-Newtonian flow in the dense liquid and gaseous states are investigated by NEMD computer simulations applied to model monatomic fluids. We use *mainly* the PUT equations of motion for shear flow, but they are implemented in a new way. We show that in non-Newtonian shear flow there appear non-vanishing correlation functions, of the generic form, $\langle v_\alpha(0)v_\beta(t)\rangle$, and $\langle P_{\alpha\beta}(0)P_{\gamma\delta}(t)\rangle$ for the soft-sphere and Lennard-Jones fluids in two and three dimensions. These correlation functions are trivially zero in the absence of shear flow. They become highly structured with shear flow and generally have a finite negative value at $t = 0$. They can exhibit time-reversal asymmetry, especially at large shear rate due to the vorticity term in the strain rate tensor.

1. Introduction

At sufficiently low shear rates the viscosity of a fluid is independent of shear rate. This viscosity is called the Newtonian viscosity. At large shear rates the viscosity of a fluid decreases further below the Newtonian viscosity with increasing shear rate. This decrease in viscosity is called shear-thinning. At still higher shear rates the viscosity of *dense fluids* increases again dramatically. This is called shear-thickening. It only occurs in dense liquids, unlike shear-thinning which is exhibited by fluids at all densities. The shear-thickening regime is associated with a highly disordered microstructure with large density fluctuations on an atomic distance scale, hence its alternative name of 'structural' turbulence. This is to distinguish it from 'kinetic' or 'convective' turbulence, exhibited by low-density gases under shear. One objective of current research is to understand the microscopic origins of these changes and the associated statistical mechanics. Our contribution, in this paper, is to use time correlation functions to characterise these non-equilibrium fluids. Time correlation functions play a central role in describing the dynamics of equilibrium and non-equilibrium states.[1,2] A shear velocity field has a pronounced effect on the time correlation functions of a simple fluid,[3,4] making them sensitive probes of non-equilibrium flow. There are certain time correlation functions that *only* have non-zero structure in the presence of shear flow, which make them particularly useful in this respect.

In this report we describe the theory that predicts those time-correlation functions (CF) existing in (symmetry breaking) simple planar shear flow, which are trivially zero in the absence of shear flow for symmetry reasons. In addition, we examine these CFs in the distinct regimes of non-Newtonian flow and the onset of turbulence in the dense liquid and gas phases.

The earliest simulations of shear flow using molecular dynamics attempted to reproduce the experimental arrangement of boundary-driven flow. The contents of the MD cell were sheared by two boundaries translating in opposing directions on opposite faces of the cell (in three dimensions). Periodic boundaries in one of the three dimensions was sacrificed to achieve this. More recent advances in non-equilibrium statistical mechanics have provided algorithms that enable shear-thinning and the onset of shear-thickening to be simulated by molecular dynamics, maintaining periodic boundary conditions in all three directions.[5,6] Of these, the SLLOD equations of motion were the first to be applied widely.[6] These equations of motion maintain the desired velocity gradient on an atomic distance scale throughout the cell. The SLLOD equations of motion produce, in extreme shear-thinning, what has come to be called the 'string' phase, in both two and three dimensions. This is so called because the molecules reorganize from an essentially random structure at zero shear rate to a new structure with long-range order. The molecules reform into lines or 'strings' along the flow direction. These strings pack into a triangular lattice, when viewed in cross-section. The strings translate with an average velocity with respect to one another, depending on their position along the velocity gradient of the flow field (y direction for a shear rate, $\partial v_x/\partial y$). The string phase is observed in sheared colloidal suspensions, but would not be observed experimentally in monatomic fluids at the necessary shear rates to produce shear-thinning. The reason for this derives from the shear rates at which similar extents of shear-thinning occur in these two systems. Colloidal fluids shear thin at shear rates $\dot\gamma \approx 1\ s^{-1}$, depending somewhat on the size of the suspending particle and its volume fraction. Monatomic fluids, in contrast, shear thin at shear rates $\approx 10^{12}\ s^{-1}$. The Reynolds number, $Re = mL^2\rho\dot\gamma/\eta$, where m is the mass of the particle, L is the separation between the shearing plates, ρ is the number density and η is the shear viscosity, predicts the conditions under which turbulence occurs. Turbulence sets in when $Re \geqslant 10^3$. For the same L we note that in the shear-thinning regime, Re is *ca.* 10^{12} larger for monatomic fluids than for colloidal suspensions.[7] Therefore, although the string phase is an intrinsic property associated with shear-thinning (and observed for colloidal dispersions), shear-thinning followed by turbulence in monatomic fluids occurs in essentially liquid-like structures with no long-range order.

In a simulation we can suppress turbulence. The SLLOD equations of motion suppress the velocity fluctuations inherent in turbulence and therefore promote and sustain these strings at shear rates at which they would be unstable in the real monatomic fluid. The effect can be demonstrated even by simulation by comparing two equations of motion that constrain the velocity fluctuations to differing extents. The strings can be dismissed by constraining the velocity profile

† Visiting Academic at RHBNC and Dept. Microelectronics and Electrical Engineering, Trinity College, Dublin 2, Ireland. Also Honorary Research Fellow, Dept. Physics, University of Lancaster, Lancaster LA1 4YB, U.K.

only on a cell-distance scale, rather than at all points within the MD cell as with SLLOD, using a profile-unbiased thermostat (PUT). Evans and Morriss showed that the PUT algorithm was capable of dispelling the 'string' phase in a two-dimensional soft-disc simulation,[6] thereby generating a more realistic representation of shear thickening for monatomic fluids. By virtue of this feature one can argue that the PUT algorithm is a more realistic model of the experimental situation than the SLLOD algorithm as it permits velocity fluctuations at least up to the distance scale of the MD cell. Nevertheless, because of their still widespread use, we apply both the SLLOD and PUT algorithms in two and three dimensions to investigate all of these non-equilibrium rheological regimes and determine their dynamical 'signatures' as measured by the new cross-correlation functions (CCFs). We note that many of the new CCFs are evident at shear rates low enough (in the mild shear-thinning regime) at which both SLLOD and PUT give indistinguishable results. It is only at shear rates large enough to produce extreme shear-thinning and shear-thickening that differences between the two equations of motion become manifest, in which case the PUT results are most realistic.

We now discuss the theory that enables us to predict those CCFs that may exist in the presence of a perturbing field.

Whiffen introduced the concept of 'Group Theoretical Statistical Mechanics' (GTSM as the application of group theory to the thermodynamic ensemble average, $\langle \ldots \rangle$.[8] Symmetry can be used to predict those averages existing and vanishing in both the laboratory-fixed frame, XYZ, and the molecule-fixed frame, xyz, applying group theory to the ensemble averages.[9,10] In a recent publication we confirmed by SLLOD NEMD the predictions of GTSM for planar couette flow, which predicts the existence of new cross-correlation functions.[11] In simple planar couette flow there appear in the laboratory frame, XYZ, cross-correlation functions between components of the atomic diffusion velocity and also others between the pressure tensor. If the strain rate is $\partial v_X/\partial Z$, the cross-correlations are of the type $\langle v_X(t)v_Z(0)\rangle$, $\langle P_{aX}(t)P_{aZ}(0)\rangle$ and $\langle P_{aa}(t)P_{XZ}(0)\rangle$, where v is the atomic velocity in the XYZ frame and $P_{\alpha\beta}$ is the $\alpha\beta$ component of the pressure tensor. This also includes those CCFs with time arguments reversed, which can be different functions at non-equilibrium. These are not incorporated in classical rheological treatments; they are, however, fundamentally important to any understanding of rheology and have so far been totally neglected. For example, they cause the Weissenberg effect, which is a flow in a direction perpendicular to the imposed strain rate. In fact, Oldroyd in his papers called these phenomena *cross*-elasticity effects without recognising the importance of the CCFs in characterising cross-effects.[12,13]

Having confirmed the validity of GTSM and the existence of these new cross-correlation functions in a recent paper,[11] we extend this study to explore specifically non-Newtonian effects. These are shear-thinning and ' structural ' turbulence (also called shear-thickening). These occur at states close to the liquid/solid coexistence line for two- and three-dimensional monatomic systems. We also investigate low-density states in three dimensions to probe the onset of kinetic or 'convective' turbulence.

This paper is organised as follows. In section 2 the GTSM theory is applied to simple planar shear or couette flow. A brief summary is made of the group-theoretical arguments leading to the prediction of new cross-correlation functions induced by $v_X(Z)$ shear flow. In section 3 the NEMD molecular dynamics models for SLLOD and PUT are described and applied to determine shear-flow time-correlation functions. Discussion of the results is given in section 4. Conclusions are presented in section 5.

2. Group Theory Statistical Mechanics

The symmetry arguments for the appearance of the shear-induced cross-correlation functions depend on group theory in the laboratory frame XYZ defined by the three-dimensional rotation–reflection group, $R_3(3)$, with irreducible representations denoted by the D symbols, $D_g^{(0)}, \ldots, D_g^{(\infty)}$ and $D_u^{(1)}, \ldots, D_u^{(\infty)}$, respectively; here the subscript, g (or *gerade*) denotes even to parity reversal symmetry, and subscript u (or *ungerade*) denotes odd to parity reversal symmetry.[14,15] The superscripts refer to the order to the spherical harmonics. In couette flow in the limit of zero strain rate

$$\Pi_{XZ} = \eta \frac{dv_X}{dZ} \tag{1}$$

where Π is the shear stress and η is the viscosity, a simple scalar of D_g^0 symmetry and the streaming velocity is $v_X(Z)$. Eqn (1) applies in the limit $dv_X/dZ \to 0$. At finite shear rate, η is a function of $\dot\gamma = dv_X/dZ$ and a more complicated stress tensor is required. In general,

$$\Pi = 2\eta(\dot\gamma)\dot\gamma. \tag{2}$$

For both eqn (1) and eqn (2) GTSM applies at steady state in the presence of shear flow, where the isotropic $R_3(3)$ symmetry of the fluid is distorted, showing up in new non-zero terms in the stress tensor. The latter is found by considering the tensor product

$$\dot\gamma = v(r^{-1}) \tag{3}$$

making up nine elements of the velocity gradient. Here, r, is the position vector whose single laboratory frame component is Z. This product has the D symmetry

$$\Gamma(v)\Gamma(r^{-1}) = D_u^{(1)}D_u^{(1)} = D_g^{(0)} + D_g^{(1)} + D_g^{(2)} \tag{4}$$

where we have used the Clebsch–Gordan theorem,[14,15]

$$D^{(m)}D^{(n)} = D^{(m+n)} + \cdots + D^{|m-n|}. \tag{5}$$

In eqn (1) and (2) the symmetry of the shear viscosity, η, is that of a scalar, $D_g^{(0)}$ having negative time-reversal symmetry. The shear stress tensor, Π, and the pressure tensor, $P(=-\Pi)$ have the symmetry, $D_g^{(0)} + D_g^{(1)} + D_g^{(2)}$. The representation, $D_g^{(0)} + D_g^{(1)} + D_g^{(2)}$, of the strain rate tensor reflects the fact that it has an antisymmetric component of vorticity, or symmetry, $D_g^{(1)}$, and a symmetric traceless component of symmetry, $D_g^{(0)} + D_g^{(2)}$. A system under shear at steady state causes the $R_3(3)$ symmetry of the equilibrium fluid to be broken by the strain rate tensor of symmetry, $D_g^{(0)} + D_g^{(1)} + D_g^{(2)}$. This makes possible the existence of ensemble averages of this symmetry according to GTSM. On the molecular scale, the strain rate tensor applied in couette flow makes possible the existence of time correlation functions of the same symmetry both in the XYZ frame and in the molecule-fixed xyz frame. (In monatomic fluids the second case is inapplicable.) The tensor symmetry of all time correlation functions of the type, $\langle A(0)A^T(t)\rangle$, where A is a polar or axial vector is also, $D_g^{(0)} + D_g^{(1)} + D_g^{(2)}$. Thus all nine elements may exist in an atomic fluid under shear. Where there is only one component of the velocity gradient in the planar couette flow, *e.g.* dv_X/dZ, then only one independent off-diagonal element of the time autocorrelation function, $\langle A(0)A^T(t)\rangle$ appears in the laboratory XYZ frame. However, this may appear in all time cross-correlation functions of this type (*i.e.* containing the X and Z superscripts) and will be the microscopic characteristic of the applied strain rate tensors. The strain rate tensor will also allow the existence in the XYZ frame of time cross-correlation functions of type, $\langle A(0)B^T(t)\rangle$, with $D_g^{(0)} + D_g^{(1)} + D_g^{(2)}$ symmetry.

In the special case of shear applied to an atomic liquid, treated in this work, the $D_g^{(0)} + D_g^{(1)} + D_g^{(2)}$ symmetry of the applied field (1) causes the off-diagonal peculiar velocity time correlation function, $\langle \bar{v}_X(0)\bar{v}_Z(t)\rangle$ to appear in the laboratory frame, along with the off-diagonal element of the pressure tensor time correlation functions, $\langle P_{XY}(0)P_{YZ}(t)\rangle$, $\langle P_{YZ}(0)P_{XZ}(t)\rangle$, $\langle P_{XZ}(0)P_{YY}(t)\rangle$ and $\langle P_{XZ}(0)P_{ZZ}(t)\rangle$. These results are appreciated recognising that, $\langle P_{XY}(0)P_{ZY}(t)\rangle$, contains the component $\langle \bar{v}_Y(0)\bar{v}_Y(t)\bar{v}_Z(0)\bar{v}_Z(t)\rangle$. The two correlation functions contained within this time average are non-zero. Similar remarks can be made for $\langle P_{YZ}(0)P_{YZ}(t)\rangle$ and $\langle P_{YZ}P_{ZZ}(t)\rangle$. In each of these cases the component velocity time correlation functions exist by symmetry. Thus the existence of $\langle \bar{v}_X(0)\bar{v}_Z(t)\rangle$ implies the existence of the above elements of the pressure tensor autocorrelation function. The full symmetry of the time correlation function of the pressure tensor in the laboratory XYZ frame is:

$$(D_g^{(0)} + D_g^{(1)} + D_g^{(2)})(D_g^{(0)} + D_g^{(1)} + D_g^{(2)}) \quad (6)$$

which, on expansion, gives

$$(D_g^{(1)} + D_g^{(2)} + D_g^{(3)} + D_g^{(4)}) + 2(D_g^{(1)} + D_g^{(2)} + D_g^{(3)}) + 3(D_g^{(0)} + D_g^{(1)} + D_g^{(2)}).$$

This includes scalar, vector and tensor symmetry up to rank (4). The CCF $\langle v_X(0)v_Z(t)\rangle$ also exists.

3. Simulation Details

In this section we describe two methods for incorporating planar shear flow in the classical equations of motion of molecular dynamics. The first method described, SLLOD, forces the molecules to flow along superposed shear flow lines. Velocity deviations from this are presumed to be caused by temperature fluctuations. These are damped out by the thermostatting process. The newer profile unbiased algorithm (PUT) was devised to eliminate this drawback, to allow more freedom for velocity fluctuations about the local flow velocity derived from the MD cell average shear rate. It is therefore more realistic at high shear rates close to the onset of turbulence. Both algorithms give the same results at low shear rates close to the Newtonian regime. The PUT algorithm is more realistic at high shear rates at which appreciable shear thinning is manifest; therefore, it is on this algorithm which we concentrate.

The three-dimensional MD simulations used particles interacting *via* the Lennard-Jones potential

$$\phi(r) = 4\varepsilon[(\sigma/r)^{12} - (\sigma/r)^6] \quad (7)$$

whereas the two-dimensional simulations were performed using the soft-sphere potential

$$\phi(r) = 4\varepsilon(\sigma/r)^{12}. \quad (8)$$

3.1 Two-dimensional Simulations

The molecular coordinates were updated in time steps of duration h, using the leapfrog recasting of the Verlet algorithm[16]

$$R_x(t + h) = R_x(t) + \Delta R_x(t), \quad (9)$$

and

$$R_y(t + h) = R_y(t) + \Delta R_y(t). \quad (10)$$

We have omitted the particle subscripts, i, for the present. At constant total energy we have

$$\Delta R_x(t) = \Delta R_x(t - h) + F_x(t)h^2/m \quad (11)$$

$$\Delta R_y(t) = \Delta R_y(t - h) + F_y(t)h^2/m \quad (12)$$

where $F_x(t)$ and $F_y(t)$ are the forces on a molecule at time t and m is the mass of the molecule (for simplicity, they all have the same mass here).

$$F_{xi} = -\sum_{i \neq j}^{N} \left.\frac{\partial \phi(r)}{\partial r}\right|_{r=r_{ij}} \quad (13)$$

where $r_{ij} = R_i - R_j$. The subscript, i, denotes the molecule index and R_i is the position of molecule i. At constant temperature, T, (which is essential for dissipative sheared fluids) we maintained constant temperature using the so-called velocity rescaling method as first derived by Woodcock[17]

$$\Delta R_x(t) = [\Delta R_x(t - h) - \bar{X}] \times K(t - h) + \bar{X} + F_x(t)h^2/m \quad (14)$$

$$\Delta R_y(t) = [\Delta R_y(t - h) - \bar{Y}] \times K(t - h) + \bar{Y} + F_y(t)h^2/m. \quad (15)$$

At this point we have introduced extra displacements, $\bar{X}$ and $\bar{Y}$, components of $\bar{R}$, which are zero at equilibrium but which will be assigned values when shear flow is introduced into the dynamics. The constant, $K(t - h)$, is a scaling factor which, under shearing conditions, is on average slightly less than unity.

$$K(t - h) = [(2N - 3)k_B T/2E_k(t - h)]^{1/2} \quad (16)$$

where $E_k(t - h)$ is the kinetic energy of the MD cell of particles

$$E_k(t - h) = \frac{1}{2}\sum_{i=1}^{N} m\dot{R}(t - h)^2 \quad (17)$$

where to an adequate approximation

$$\dot{R} = [\Delta R(t - h) - \bar{R}]/h. \quad (18)$$

Boundary-driven shear flow was implemented using so-called Lees–Edwards periodic boundary conditions.[18] These are written succinctly as

$$\dot{R}_x^i = \dot{R}_x + n_y^i L_y \dot{\gamma} \quad (19)$$

$$\dot{R}_y^i = \dot{R}_y \quad (20)$$

where the superscript i refers to the image of the particle whose position in the 'real' MD cell is R. The value of n_i^y (the image cell index) in the y-direction is in the range $-\infty < n_i^y < \infty$. The real MD cell corresponds to $n_i^y = 0$. The side-length of the MD cell in the y direction is L_y. The position displacements derived from eqn (19) and (20) are

$$R_x^i = R_x + n_i^y L_y \dot{\gamma} t + n_i^x L_x \quad (21)$$

$$R_y^i = R_y + n_i^y L_y \quad (22)$$

where t is the time duration of the simulation since the application of the shear velocity field. The range of values of n_i^x, the image cell index in the x-direction, is $-\infty < n_i^x < \infty$. If the 'real' particle at R moves out of the cell, its image i enters at the position

$$R_x \rightarrow \{R_x + n_i^y L_y \dot{\gamma} t + n_i^x L_x\} \quad (23)$$

$$R_y \rightarrow \{R_y + n_i^y L_y\}. \quad (24)$$

The notation $\{\ldots\}$ denotes the application of periodic boundary conditions so that R_x^i falls within the same limits as that of R_x (*i.e.* $0 < R_x^i < L_x$, where L_x is the side-length of the MD cell in the x direction).

The thermostatting method distinguishes SLLOD from PUT. In SLLOD a linear velocity profile $v_X(Z)$ is assumed in the thermostatting procedure. Any deviations from this will be taken as an extra contribution to the temperature and duly suppressed. In PUT no assumption is made about the instantaneous velocity distribution within the MD cell. However, by virtue of the Lees–Edwards boundary conditions, the flow on distance scales of the order of L_y is forced

to be linear couette. In eqn (14), (15) and (18), for SLLOD

$$\bar{X} = R_y \dot{\gamma} h, \tag{25}$$

and $\bar{Y} = 0$. For PUT

$$\bar{X}_i = (\Delta R_{xi} + \sum_{j \neq i}^{n_c^i} \Delta R_{xj})/(n_c^i + 1), \tag{26}$$

$$\bar{Y}_i = (\Delta R_{yi} + \sum_{j \neq i}^{n_c^i} \Delta R_{yj})/(n_c^i + 1), \tag{27}$$

where n_c^i are all those molecules within a radius r_p of the centre of molecule i. We adopted two values of r_p: 1.5σ and 2.0σ.

Our implementation of the PUT equations of motion differs from that of Evans and Morriss. We believe this new method is more realistic in maintaining the local circular (2D) or spherical (3D) symmetry of the fluids. In both cases a local temperature for molecule i is defined with respect to a 'local' drift velocity. The difference between the two approaches lies in the method for evaluating the local drift velocity. Evans and Morriss partitioned the MD cell into sub-boxes. The average drift velocity within each sub-box was calculated. This was then used to determine the temperature of each particle in the cell. However, we did not use such a procedure to obtain the temperature of each particle. Rather, a local drift velocity was determined for each molecule by taking a circular truncation radius and finding the average velocity within the disc. This is straightforwardly performed in the forces double loop of the program and does not slow the program significantly. We suggest that our treatment is more realistic (*i.e.* less constrained). This we rationalise as follows. Using the subcell method there is a driving force biasing the density of each subcell to be that of the average density of the whole MD cell. This is because subcells with fewer molecules than the average will be effectively 'colder' than the mean temperature. Similarly, subcells with more particles than the average will be 'hotter' than the average. There will be compensating drifts of particles from hot to cold subcells to correct any temporary imbalance of numbers of molecules. In the present implementation of PUT there is no implicit space-fixed grid for thermostatting purposes. Therefore, density fluctuations are allowed to occur naturally in this implementation of PUT.

We calculated the viscosity, η, from

$$\eta = -P_{xy}/\dot{\gamma} \tag{28}$$

where

$$P_{xy} = \frac{1}{A}\left(\sum_{i=1}^{N} m_i \tilde{v}_{xi}\tilde{v}_{yi} - \sum_{i=1}^{N-1}\sum_{j>1}^{N} (r_{xij} r_{yij}/r_{ij}) \frac{\mathrm{d}\phi(r_{ij})}{\mathrm{d}r}\right) \tag{29}$$

and $\tilde{v}_\alpha$ is the peculiar velocity (*i.e.* that in excess of the streaming flow velocity), r_{xij} is the x component of r_{ij} and $A = (N/\rho)$, the area of the MD cell.

3.2 Three-dimensional Simulations

The basics of the three-dimensional simulations have been described elsewhere.[19] The MD simulations were performed on cubic unit cells of volume V containing $N = 108$ and $N = 500$ Lennard-Jones (LJ) particles of mass m. The interactions were truncated at 2.5σ. A large time-step version of the Verlet algorithm was used to increment the positions of the molecules,[20] in the case of the SLLOD simulations. We use LJ reduced units throughout, *i.e.* $k_B T/\varepsilon \rightarrow T$ and number density $\rho = N\sigma^3/V$. Time is in $\sigma(m/\varepsilon)^{1/2}$, shear rate is in $(\varepsilon/m)^{1/2}/\sigma$, viscosity is in $(m\varepsilon)^{1/2}/\sigma^2$ and stress is in $\varepsilon\sigma^{-3}$. (Note that in two dimensions η has units of $(m\varepsilon)^{1/2}/\sigma$ and stress has units of $\varepsilon\sigma^{-2}$). Two state points were examined. There was a near triple-point state, at $\rho = 0.8442$ and $T = 0.722$. A low-density state, $\rho = 0.1$ and $T = 2.5$, was also examined. At this density the shear viscosity is dominated by the kinetic component, η_k. The PUT algorithm was implemented as a straightforward extension of the two-dimensional method. For SLLOD a previously described formulation was used.[4,20] As before, the peculiar or thermal velocity is denoted by $\tilde{v}_\alpha$. The SLLOD equations of motion are written in as two first-order equations

$$\dot{R}_X = v_X = \tilde{v}_X + \dot{\gamma} R_Z \tag{30}$$

$$\dot{R}_Y = v_Y = \tilde{v}_Y \tag{31}$$

$$\dot{R}_Z = v_Z = \tilde{v}_Z \tag{32}$$

$$\frac{\mathrm{d}\tilde{v}_X}{\mathrm{d}t} = F_X/m - \dot{\gamma}\tilde{v}_Z - \beta\tilde{v}_X \tag{33}$$

$$\frac{\mathrm{d}\tilde{v}_Y}{\mathrm{d}t} = F_Y/m - \beta\tilde{v}_Y \tag{34}$$

$$\frac{\mathrm{d}\tilde{v}_Z}{\mathrm{d}t} = F_Z/m - \beta\tilde{v}_Z \tag{35}$$

where the α component of the force on a particle is F_α, the velocity is V_α, the peculiar α velocity component is $\tilde{v}_\alpha$, and β is the coefficient in the Gaussian isokinetic thermostatting control.[19]. (We were not able to cast the PUT algorithm into two first-order differential equations with Gaussian isokinetic thermostatting. This scheme, eqn (30)–(35) was possible with SLLOD.)

The quantity, $\tilde{R}_\alpha$, a 'peculiar' position, measures the distance moved from internal forces only, $\tilde{R}_\alpha(t) = R_\alpha(t) - R_\alpha(0)$, neglecting the streaming component

$$\tilde{R}_\alpha(t) = \int_0^t \tilde{v}_\alpha(t')\,\mathrm{d}t'. \tag{36}$$

Computations were carried out on a CRAY-1S at the University of London Computer Centre.

4. Results and Discussion

A summary of the two- and three-dimensional simulations performed is given in table 1. This also incorporates the normal pressures and shear viscosities obtained from each simulation.

In three-dimensions, we evaluated the correlation functions,

$\langle\tilde{v}_X(0)\tilde{v}_X(t)\rangle$, $\langle\tilde{v}_Y(0)\tilde{v}_Z(t)\rangle$, $\langle\tilde{v}_Y(0)\tilde{v}_X(t)\rangle$, $\langle\tilde{v}_Z(0)\tilde{R}_X(t)\rangle$,
$\langle\tilde{v}_Y(0)\tilde{R}_X(t)\rangle$, $\langle\tilde{v}_Z(0)\tilde{R}_Y(t)\rangle$, $(V/k_B T)\langle P_{XY}(0)P_{XY}(t)\rangle$,
$(V/k_B T)\langle P_{XZ}(0)P_{XZ}(t)\rangle$, $(V/k_B T)\langle P_{YZ}(0)P_{YZ}(t)\rangle$,
$(V/k_B T)\langle P_{XZ}(0)P_{YZ}(t)\rangle$, $(V/k_B T)\langle P_{XZ}(0)P_{XY}(t)\rangle$,
$(V/k_B T)\langle P_{XY}(0)P_{YZ}(t)\rangle$, $(V/k_B T)\langle P_{XZ}(0)P_{XX}(t)\rangle$,
$(V/k_B T)\langle P_{XX}(0)P_{YY}(t)\rangle$ and $(V/k_B T)\langle P_{XX}(0)P_{ZZ}(t)\rangle$.

GTSM predicts that the following correlation functions could exist in $\mathrm{d}v_X/\mathrm{d}Z$ shear flow: $\langle\tilde{v}_X(0)\tilde{v}_X(t)\rangle$, $\langle\tilde{v}_X(0)\tilde{R}_X(t)\rangle$, $\langle\tilde{v}_Y(0)\tilde{v}_Z(t)\rangle$, $\langle\tilde{v}_Z(0)\tilde{R}_Z(t)\rangle$, $(V/k_B T)\langle P_{XY}(0)P_{YZ}(t)\rangle$, $(V/k_B T)\langle P_{XZ}(0)P_{XX}(t)\rangle$, $(V/k_B T)\langle P_{XZ}(0)P_{YY}(t)\rangle$ and $(V/k_B T)\langle P_{XZ}(0)P_{ZZ}(t)\rangle$. We observed all of these as non-zero functions and also the different CCFs formed by reversing the time arguments in the above CCFs. In two-dimensions the cross-correlation functions of the above form with only X and Y components were evaluated. The existence of the

Table 1. Summary of the NEMD simulations[a]

	D	ρ	T	N	h	$\dot{\gamma}$		$N_T/1000$	$P_{xx}P_{yy}$	P_{zz}	η_k	η
S[b]	2	0.73322	1.0	896		0.267	8.73	8.73	8.73	—	0.124	2.78
P	2	0.73322	1.0	882	0.0075	0.267	4	9.49	9.49	—	0.079	2.691
P	2	0.73322	1.0	882	0.0005	2	4	20.57	21.40	—	0.079	1.767
P	2	0.73322	1.0	882	0.003	2	4	11.77	12.09	—	0.079	1.643
S	2	0.73322	1.0	882	0.001	5	4	8.71	13.46	—	0.056	0.447
P	2	0.73322	1.0	882	0.001	5	8	19.94	25.88	—	0.053	1.269
P	2	0.73322	1.0	882	0.001	5	8	11.59	19.70	—	0.065	0.779
S[b]	2	0.73322	1.0	896		8.9		8.75	51.2	—	0.062	1.02
P	2	0.73322	1.0	882	0.001	10	4	49.61	65.71	—	0.025	1.374
P	2	0.73322	1.0	882	0.001	10	8	54.45	70.60	—	0.027	1.635
P*	2	0.73322	1.0	882	0.001	10	8	81.96	108.93	—	0.032	3.210
S	2	0.73322	1.0	882	0.001	10	8	8.66	13.68	—	0.016	0.180
P	2	0.73322	1.0	882	0.00025	17.82	4	521.98	500.20	—	0.018	10.32
P	2	0.73322	1.0	882	0.00015	17.82	8	728.96	720.00	—	0.019	15.46
S	2	0.73322	1.0	882	0.0003	17.8	8	6.75	12.26	—	0.022	0.052
S	3	0.1	2.5	108	0.0075	0	200	0.24	0.24	0.23	—	—
S	3	0.1	2.5	500	0.003	0	20	0.25	0.25	0.25	—	—
P*	3	0.1	2.5	500	0.004	0	20	0.27	0.25	0.25	—	—
S	3	0.1	2.5	108	0.0075	1	600	0.36	0.17	0.17	0.132	0.149
S	3	0.1	2.5	108	0.0075	1	600	0.36	0.17	0.17	0.132	0.149
S	3	0.1	2.5	500	0.003	1	20	0.39	0.18	0.18	0.141	0.157
P*	3	0.1	2.5	500	0.002	1	20	0.48	0.13	0.13	0.048	0.055
S	3	0.1	2.5	500	0.003	5	20	0.56	0.08	0.12	0.034	0.044
P*	3	0.1	2.5	500	0.003	5	20	0.58	0.09	0.09	0.014	0.024
S	3	0.1	2.5	500	0.003	10	20	0.63	0.08	0.18	0.019	0.028
P*	3	0.1	2.5	500	0.002	10	40	0.64	0.05	0.05	0.0056	0.0096
P*	3	0.1	2.5	500	0.0015	20	30	0.66	0.03	0.02	0.0027	0.0036
P	3	0.8442	0.722	108	0.0075	0	200	0.31	0.31	0.33	—	—
S	3	0.8442	0.722	108	0.0075	0	28	0.03	0.02	0.01	—	—
S	3	0.8442	0.722	108	0.0075	0	700	0.03	0.02	0.02	—	—
S	3	0.8442	0.722	108	0.0075	1	20	1.12	0.75	1.22	0.0779	2.08
S	3	0.8442	0.722	108	0.0075	1	40	1.17	0.79	1.26	0.075	2.08
S	3	0.8442	0.722	108	0.0075	1	440	1.15	0.78	1.25	0.075	2.08
S	3	0.8442	0.722	108	0.0075	1	610	1.15	0.78	1.25	0.075	2.07 (5)
S	3	0.8442	0.722	108	0.0075	1	600	1.17	0.79	1.25	0.075	2.08
P	3	0.8442	0.722	108	0.0075	1	800	1.50	1.15	1.59	0.072	2.06
P	3	0.8442	0.722	500	0.0075	1	30	1.61	1.31	1.73	0.0744	2.11
S	3	0.8442	0.722	500	0.0075	1	20	1.22	0.90	1.35	0.0801	2.11
S	3	0.8442	0.722	108	0.0075	3	200	1.93	1.29	2.24	0.0542	0.88
S	3	0.8442	0.722	500	0.0075	3	20	−0.18	−0.30	−0.02	0.0589	0.66
P	3	0.8442	0.722	108	0.0075	3	200	3.51	2.55	3.82	0.0590	1.19
P	3	0.8442	0.722	500	0.0075	3	40	4.67	3.54	5.33	0.0641	1.49
P	3	0.8442	0.722	500	0.0075	3	20	2.72	2.10	4.26	0.0631	1.10
P	3	0.8442	0.722	500	0.003	10	20	−0.49	0.36	3.99	0.0234	0.126
P	3	0.8442	0.722	500	0.002	20	20	−1.25	−1.85	−0.56	0.0031	0.0112
P*	3	0.8442	0.722	500	0.002	20	20	−1.07	1.89	8.20	0.0029	0.0143
P*	3	0.8442	0.722	500	0.002	20	30	−1.14	2.00	8.57	0.0029	0.0138
S	3	0.8442	0.722	500	0.003	20	20	−0.17	0.69	2.42	0.0169	0.0486
S	3	0.8442	0.722	500	0.003	20	20	0.71	0.26	2.03	0.0171	0.0468

[a] P denotes the PUT algorithm with $r_s = 1.5\sigma$ and P* denotes the PUT algorithm with $r_s = 2.0\sigma$. S denotes the SLLOD algorithm. D denotes the dimension. N is the number of molecules in the MD cell of volume V. N_T is the number of time steps of duration h. η_k is the kinetic component of the viscosity. η is the total viscosity. The normal pressure components are P_{xx}, P_{yy} and P_{zz}, respectively. The shear rate is $\dot{\gamma}$. All units are LJ units although the two-dimensional simulations were performed with the SS potential [eqn (8)]. To convert quantity X in LJ units to SS units $\phi(r) = \epsilon(\sigma/r)^{12}$ then multiply by the factors: 0.8909, 1.2599, 1.12246, 0.8909 and 1.12446 for time, pressure tensor components, viscosity, distance and shear rate, respectively. [b] Ref. (3).

correlation function is independent of the use of $\bar{v}_a$ or v_a. We chose to use $\bar{v}_a$.

We first consider the three-dimensional simulations performed for high density near the LJ triple-point state. We consider the time correlation function, $\langle \bar{v}_x(0)\bar{v}_x(t)\rangle$, which in the absence of shear flow is zero at all times, t. In Fig. 1, $\langle \bar{v}_x(0)\bar{v}_x(t)\rangle$ is given for SLLOD and PUT algorithms for $\dot{\gamma} = 1.0$. As for all these field-induced CCFs they start at $t = 0$ from a value more negative than their limiting value as $t \to \infty$. At $\dot{\gamma} = 1$ there is little difference between the two algorithms. The similarity between the associated shear viscosities, revealed in table 1, supports the view that the two algorithms are producing essentially the same non-Newtonian state point. However, at progressively increasing shear rate differences appear in the CCFs produced by SLLOD and PUT. The former are generally more structured. This is because the dynamics are more 'constrained' by SLLOD than PUT (the x-component of velocity is steered continuously to $y\partial v_x/\partial y$) so that the system exists in a more confined region of phase space. PUT equations of motion are more realistic at these extremely high shear rates when arbitrarily large deviations in v_x about the continuum value are allowed.

We now consider a shear rate that manifests extreme shear-thinning by two orders of magnitude. The $\langle P_{xy}(0)P_{yz}(t)\rangle$ and $\langle P_{yz}(0)P_{xy}(t)\rangle$ for the PUT three-

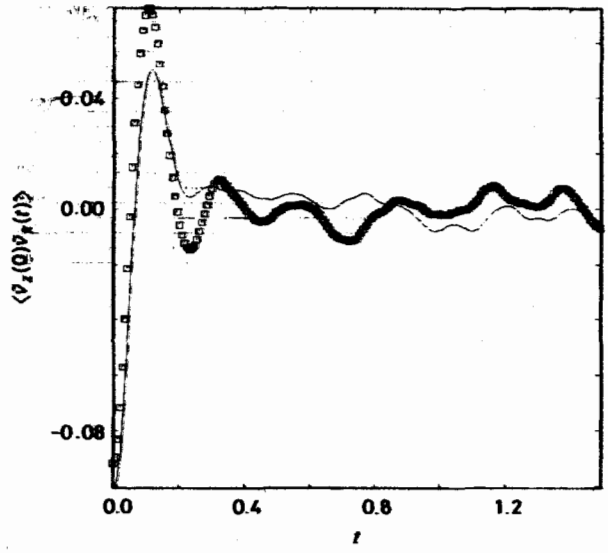

Fig. 1. The time correlation function $\langle \bar{v}_x(0)\bar{v}_y(t)\rangle$ using SLLOD (solid line) and PUT (squares) at the three-dimensional state: $\rho = 0.8442$, $T = 0.722$ and $\dot{\gamma} = 1.0$; $N = 500$.

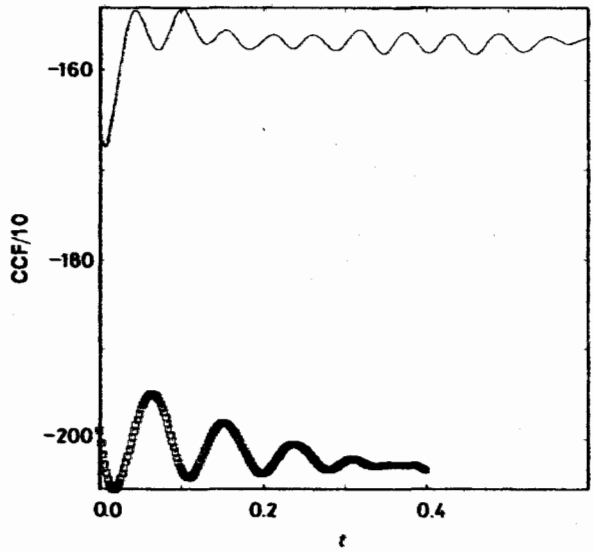

Fig. 3. The time correlation function $(V/k_B T)\langle P_{YX}(0)P_{ZX}(t)\rangle$ for SLLOD (solid line) and PUT (square symbols) at the three-dimensional state $\rho = 0.8442$, $T = 0.722$ and $\dot{\gamma} = 20.0$; $N = 500$.

dimensional LJ $\rho = 0.8442$, $T = 0.722$, $\dot{\gamma} = 20.0$ and $N = 500$ state are shown in Fig. 2. They both start from a finite negative value and then decay in an oscillatory manner with frequency $\nu \approx \dot{\gamma}$. This oscillatory structure we attribute to the formation of a 'string' phase in which the molecules travel along the streamlines in lines packed together in a triangular lattice when viewed in cross-section [see fig. 4(c), later]. Adjacent molecules in neighbouring strings are separated by a distance of the order of σ. The relative velocity between these molecules in the streaming direction is $\approx \sigma\dot{\gamma}$. Hence the frequency of registry of molecules is $\approx \dot{\gamma}$. The time-reversed function $\langle P_{YZ}(0)P_{XY}(t)\rangle$, is quite different, having an apparent negative parity to time when compared with $\langle P_{XY}(0)P_{YZ}(t)\rangle$. This can be traced to the contribution of the vorticity component of the flow, which unlike the pure strain component of the strain rate tensor, causes negative parity to time reversal. In fig. 3, $\langle P_{YZ}(0)P_{ZZ}(t)\rangle$ from the same state point is shown for SLLOD and PUT. All the $\langle P_{YZ}(0)P_{\alpha\alpha}(t)\rangle$ are non-zero in SLLOD and PUT. The SLLOD equations of motion show again a more structured CCF. In the absence of shear these CCFs are trivially zero at all times.

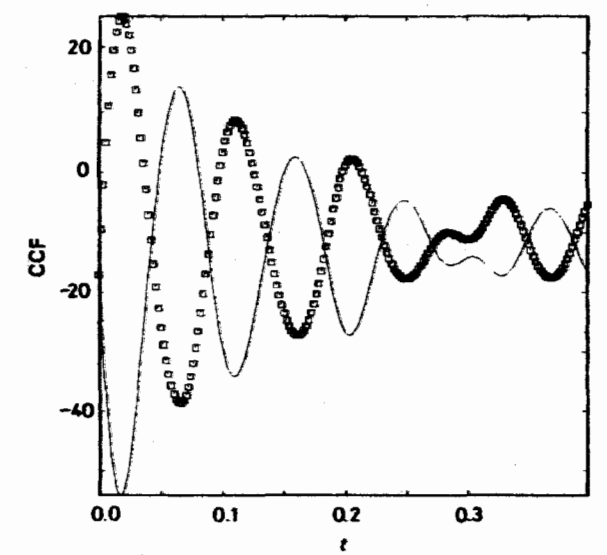

Fig. 2. The time correlation function $(V/k_B T)\langle P_{XY}(0)P_{YZ}(t)\rangle$, solid line and $(V/k_B T)\langle P_{YZ}(0)P_{XY}(t)\rangle$, squares, using PUT at the three-dimensional LJ state: $\rho = 0.8442$, $T = 0.722$ and $\dot{\gamma} = 20.0$; $N = 500$.

Fig. 4 shows the development of fluid structure from an essentially amorphous state at $\dot{\gamma} = 1.0$ through to a two-phase region at $\dot{\gamma} = 3.0$ to a full string phase at $\dot{\gamma} = 20$. Both the SLLOD and the PUT algorithms give essentially the same behaviour. This was obtained for PUT using $r_p = 1.5$ and 2.0, and was therefore independent of the number of neighbouring molecules used to define a local drift velocity. The string phase is more stable with PUT than SLLOD as it shows straighter strings. In the $\dot{\gamma} = 20.0$ SLLOD simulation strings more often buckle and 'snap'. We note that in three dimensions the PUT equations of motion produced a stable string phase for periodically repeating cells of *ca.* 500 molecules. The string phase is dispelled in two dimensions by replacing SLLOD by PUT equations of motion. This work reveals that this is not observed in three dimensions. In the $N \rightarrow \infty$ limit the string phase cannot be stable for monatomic fluids because of the large Reynolds Number associated with the shear rate used.[6] This behaviour is totally different to what is observed in two dimensions, where no evidence of a string phase is seen from PUT.[5,6] The appearance of a stable string phase obviously depends strongly on the dimension of the space for finite periodic PUT systems.[21] Although an improvement on SLLOD, the PUT equations of motion still produce the string phase in three dimensions for finite periodic systems. The periodic boundary conditions appear to have a more important role in three than in two dimensions in stabilising the string phase. The dimensions of the MD cell are significantly smaller in three than in two dimensions for the same value of N. Consequently, one needs to consider much larger N in three dimensions than in two dimensions in order to achieve comparable MD cell side-lengths.

We now consider those correlation functions from the low-density gas state. At low density there is no string phase so that many of the distinctive features associated with shear-thinning at liquid density are lost. The CCFs become shorter ranged. The same new CCFs do appear in the gas phase, again manifesting time irreversibility. The SLLOD CCFs are

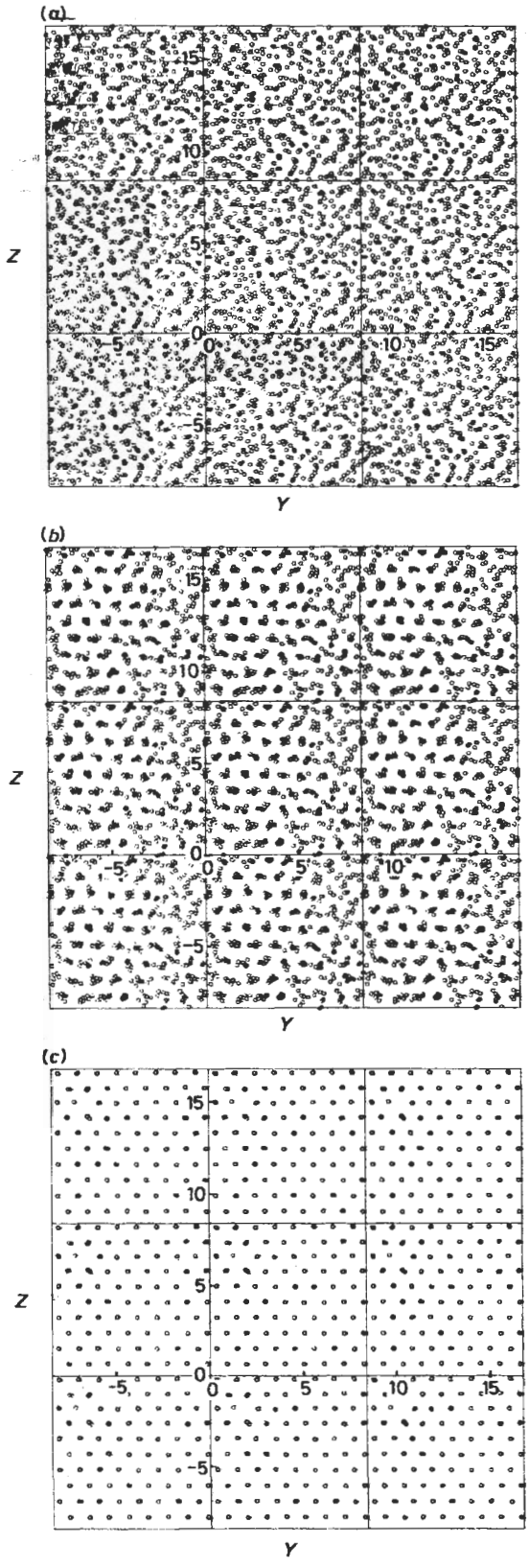

Fig. 4. Scattergrams for three-dimensional sheared LJ fluids at the three-dimensional state $\rho = 0.8442$, $T = 0.722$, $N = 500$ and a range of $\dot{\gamma}$ using the PUT algorithm. The projections of the centres of the LJ particles onto the YZ plane are shown. To facilitate the observation of any long-range structure, the real MD cell and surrounding eight images are given. (*a*) $\dot{\gamma} = 1.0$, $r_p = 1.5$; (*b*) $\dot{\gamma} = 3.0$; (*c*) $\dot{\gamma} = 20.0$, $r_p = 2.0$.

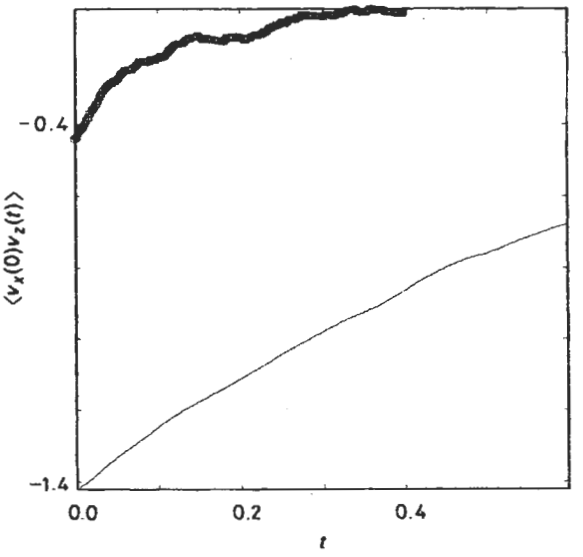

Fig. 5. The time correlation function $\langle \tilde{v}_X(0)\tilde{v}_Z(t)\rangle$ using SLLOD (solid line) and PUT (squares) at the three-dimensional LJ state; $\rho = 0.1$, $T = 2.5$ and $\dot{\gamma} = 1.0$; $N = 500$.

more pronounced but basically have the same form, as shown in fig. 5 for $\langle \tilde{v}_X(0)\tilde{v}_Z(t)\rangle$. The $\langle P_{XY}(0)P_{YZ}(t)\rangle$ function is the most pronounced and structured of all the new stress CCFs at low density. It increases in amplitude with increasing $\dot{\gamma}$. It obviously reflects the microscopic mechanism of shear stress relaxation closely and decays to zero as $t \to \infty$, whereas the $\langle P_{XZ}(0)P_{\alpha\alpha}(t)\rangle$ are more insensitive in this respect, showing a small time dependence about the means, $\langle P_{XZ}\rangle\langle P_{\alpha\alpha}\rangle$ which could be difficult to resolve experimentally.

As at high density the structures of the high shear rate fluids are different for SLLOD and PUT, the latter promotes the formation of droplets, as shown in fig. 6. (The corresponding SLLOD scattergram shows a random distribution of points.) The droplet formation is manifest also in a major decrease in viscosity, when compared with the corresponding SLLOD state, as revealed in table 1. (Small clusters do appear in SLLOD states at densities of *ca.* 0.01 at these shear rates.[22]) We note that sheared colloidal particles also aggregate in compact clusters.[23]

We now consider the two-dimensional fluids. The soft-sphere density and temperature chosen were the same as for earlier reports using SLLOD and PUT. We used $N = 882$ instead of the $N = 896$ soft-discs in the earlier treatments. Otherwise the density and temperature are the same.[6]

We find, in fig. 7, that the SLLOD equations of motion shear thin accompanied by the formation of a two-dimensional string phase (lines of atoms flowing along the streaming direction, stacked against each other at a separation of approximately one molecular diameter). The PUT systems manifest no string phase, in agreement with previous work.[6,24] However, the amorphous structure produced shows greater density fluctuations in the cell (proved to be reversible by ascending and descending shear rate) than in the implementation of PUT in ref. (6). The cavitation observed and shear-thickening is typical of experimental shear-thickening suspensions. We therefore suggest that our implementation of the PUT principle is more realistic. It must be recognised, however, that, unlike Gaussian thermostatted SLLOD, there is no unique prescription for a profile-unbiased thermostat, as there is freedom in defining the local 'drift' velocity from which the local temperature is derived.

The two-dimensional correlation functions are qualitatively the same as in the dense three-dimensional state. The

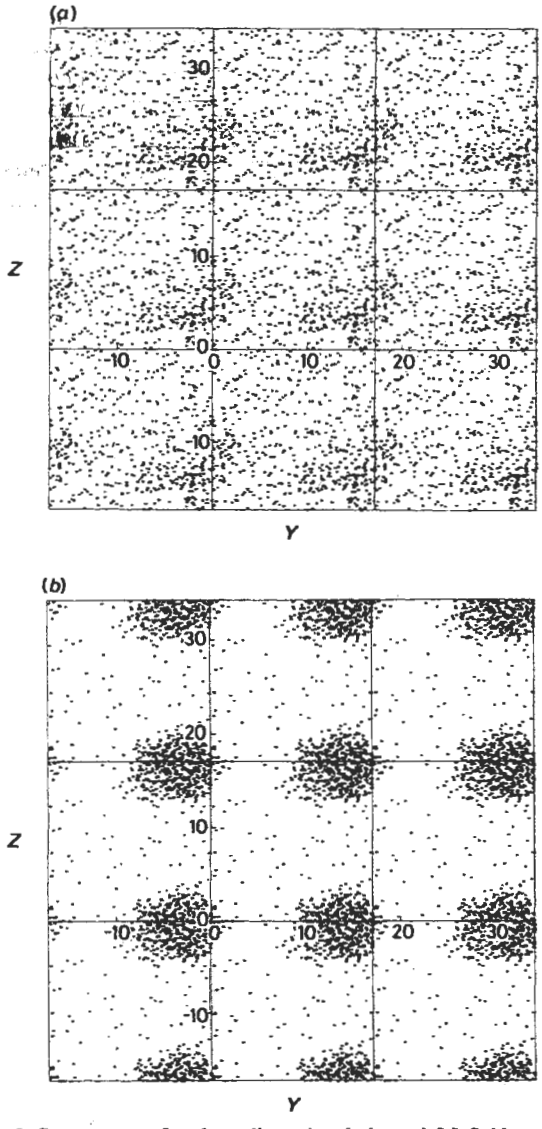

Fig. 6. Scattergrams for three-dimensional sheared LJ fluids at the three-dimensional state: $\rho = 0.1$, $T = 2.5$, $N = 500$ and a range of $\dot{\gamma}$ for the PUT algorithm. The presentation is as for fig. 4. (*a*) $\dot{\gamma} = 1.0$, $r_p = 2.0$, (*b*) $\dot{\gamma} = 5.0$, $r_p = 2.0$.

$\langle \tilde{v}_X(0)\tilde{v}_Y(t)\rangle$ start from a negative value and ascend to zero. An example of this function for the PUT $\dot{\gamma} = 17.8$ state is given in fig. 8, together with its time-reversed complement function $\langle \tilde{v}_Y(0)\tilde{v}_X(t)\rangle$. The function, $\langle P_{\alpha\alpha}(t)P_{XY}(0)\rangle$, also reveals considerable short-time structure, e.g. for $\alpha = X$ in fig. 9.

These CCFs could provide 'signatures' of the various stages of non-Newtonian behaviour (shear-thinning and -thickening) which could be measured by spectroscopy. There is strong evidence that MD can be employed to model these states. A number of recent MD simulations of 'microscale hydrodynamics' have shown that it is possible to simulate the onset of turbulence at a molecular level, looking at flow around a microscopic observation.[25] There, stationary eddy formation, wake oscillations and von Karman vortex street shedding were observed in a two-dimensional fluid of repulsive particles.

An examination of the three-dimensional CCFs reveals that although $\langle \tilde{v}_X(0)\tilde{v}_Z(t)\rangle$ and $\langle P_{XY}(0)P_{YZ}(t)\rangle$ are zero in the absence of shear they manifest an increasingly strong amplitude as shear rate rises. For example, in the three-

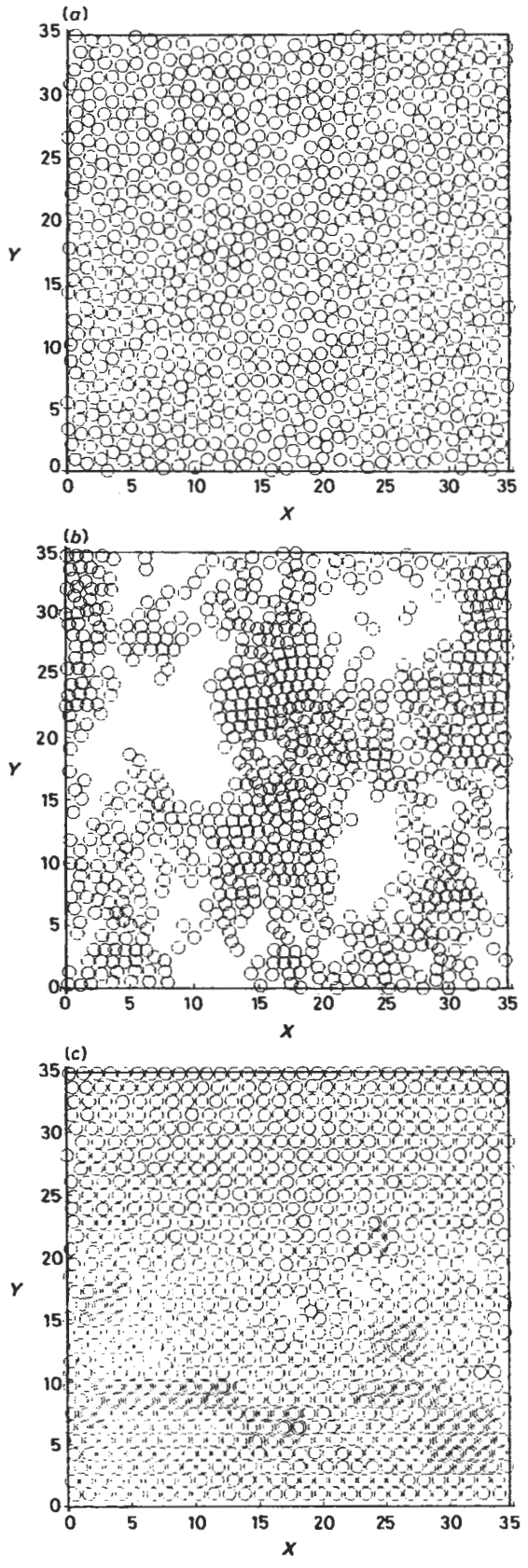

Fig. 7. Scattergrams for two-dimensional sheared LJ fluids at the SS state: $\rho = 0.7332$, $T = 1.0$, $N = 882$ and a range of $\dot{\gamma}$ for SLLOD and PUT algorithms. Shown are the SS particles represented on the XY plane as discs of diameter σ. (*a*) PUT, $\dot{\gamma} = 0.2627$, $r_p = 1.5$; (*b*) PUT, $\dot{\gamma} = 17.8$, $r_p = 1.5$, $h = 0.001$; (*c*) SLLOD, $\dot{\gamma} = 17.8$.

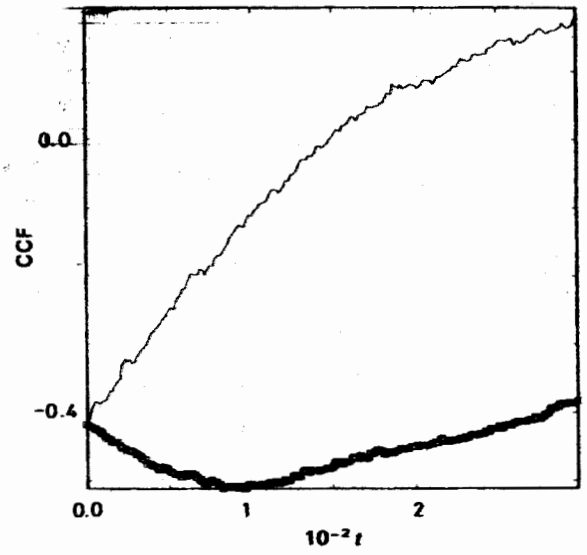

Fig. 8. The time correlation function $\langle v_x(0)v_z(t)\rangle$, square symbols, and $\langle v_z(0)v_x(t)\rangle$, solid line, for the two-dimensional SS states: $\rho = 0.733$, $T = 1.0$ and $\dot{\gamma} = 17.8$ using the PUT algorithm with $r_p = 1.5$.

dimensional gas state, $\langle v_x(0)v_x(0)\rangle$ has the values of 0.00, −0.44 and −0.75 at $\dot{\gamma} = 0.0$, 1.0 and 5.0, respectively, using the PUT algorithm ($r_p = 2.0\sigma$). The corresponding SLLOD values are 0.00, −1.42 and −1.71, being somewhat larger but following the same qualitative trend. The associated values of $[V/(k_B T)]\langle P_{xy}(0)P_{yz}(0)\rangle$ are for PUT 0.00, −0.23 and −1.19. These values are of the same order of magnitude as the fluctuations in the diagonal elements of the stress tensor so should be experimentally observable. The near triple-point state-point follows a similar trend, *e.g.* $\langle \tilde{v}_x(0)\tilde{v}_z(0)\rangle$ are −0.09, −0.23 and −0.07 at $\dot{\gamma} = 1$, 3 and 20, respectively, for PUT ($r_p = 1.5\sigma$) and the $[V/(k_B T)]\langle P_{xy}(0)P_{yz}(0)\rangle$ are −8.4, −29.6 and −17.0. (The fluctuations are somewhat larger in the two-phase regime at $\dot{\gamma} = 3$.) As the dense three-dimensional fluid results apply to a string phase, these trends are most applicable to dense colloidal suspensions which can manifest the string phase. The string phase is not produced in two dimensions. In the two-dimensional systems, $\langle \tilde{v}_x(0)\tilde{v}_y(0)\rangle$ are −0.03, −0.21 and −0.42 for $\dot{\gamma} = 0.267$, 2.000 and 20.0, respectively, through the structural turbulence transition. Therefore the amplitudes of these CCFs are roughly proportional to the extent of shear-thinning and -thickening in both SLLOD and PUT simulations.

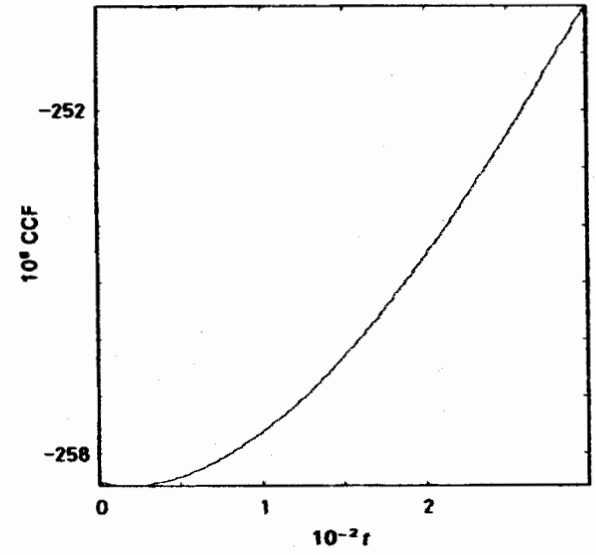

Fig. 9. The time correlation function $(V/k_B T)\langle P_{xy}(0)P_{xx}(t)\rangle$ for the two-dimensional PUT state: $\rho = 0.733$, $T = 1.0$ and $\dot{\gamma} = 17.8$ with $r_p = 1.5$.

4. Conclusions

In this paper we have established the link between a macroscopic applied field symmetry and the precise symmetry of the induced time correlation functions. We have looked at planar couette shear flow, showing that there are new time correlation functions in both the Cartesian and peculiar frames of reference. Despite present limitations on the available simulation techniques we show that these time correlation functions are shown to be sensitive probes of the magnitude of the microscopic shear rate and also to the presence of long-range order. This offers evidence that ultimately they could be used to probe non-Newtonian flow spectroscopically.

We describe a new implementation of the PUT equations of motion that produces more realistic states at high shear rates in the shear-thickening regime in two dimensions. (In three dimensions we obtained the string phase.) We also observe shear-induced droplet formation in the gaseous state, similar to that created in sheared colloidal suspensions.

D.M.H. gratefully thanks The Royal Society for the award of a Royal Society 1983 University Research Fellowship. M.W.E. thanks RHBNC for an academic visitor award. We thank S.E.R.C. for the award of computer time at the University of London Computer Centre, and the RHBNC Computer Centre for use of their VAX 11/780 computer facilities.

References

1 D. J. Evans, *Phys. Rev. A*, 1987, **36**, 4515.
2 D. J. Evans and G. P. Morriss, *Mol. Phys.*, 1987, **61**, 1151.
3 D. M. Heyes, G. P. Morriss and D. J Evans, *J. Chem. Phys.*, 1985, **83**, 4760.
4 D. M. Heyes, *Mol. Phys.*, 1986, **57**, 1265.
5 D. J. Evans and G. P. Morriss, *Phys. Rev. A*, 1984, **30**, 1528.
6 D. J. Evans and G. P. Morriss, *Phys. Rev. Lett.*, 1986, **56**, 2172.
7 D. M. Heyes, *J. Chem. Soc., Faraday Trans. 2*, 1986, **82**, 1365.
8 D. H. Whiffen, *Mol. Phys.*, 1988, **63**, 1053.
9 M. W. Evans, *Chem. Phys. Lett.*, 1988, **33**, 152.
10 M. W. Evans, *J. Phys. Chem.*, 1988, in press.
11 M. W. Evans and D. M. Heyes, *Mol. Phys.*, 1988, **65**, 1441.
12 J. G. Oldroyd, *Proc. R. Soc. London, Ser. A*, 1950, **200**, 523.
13 J. G. Oldroyd, *Proc. R. Soc. London, Ser. A*, 1958, **245**, 278.
14 R. L. Flurry Jr, *Symmetry Groups, Theory and Applications* (Prentice Hall, Englewood Cliffs, 1980).
15 R. M. Hochstrasser, *Molecular Aspects of Symmetry* (W. A. Benjamin, New York, 1966).
16 L. Verlet, *Phys. Rev.*, 1967, **98**, 159.
17 L. V. Woodcock, *Chem. Phys. Lett.*, 1971, **10**, 257.
18 A. W. Lees and S. F. Edwards, *J. Phys. C*, 1972, **5**, 1921.
19 K. D. Hammonds and D. M. Heyes, *J. Chem. Soc., Faraday Trans. 2*, 1988, **84**, 705.
20 D. MacGowan and D. M. Heyes, *Mol. Sim.*, 1988, **1**, 277.
21 Discovered simultaneously by W. Loose, private communication.
22 D. M. Heyes and R. Szczepanski, *J. Chem. Soc., Faraday Trans. 2*, 1987, **83**, 319.
23 E. Guyon, in *Les Houches Session XLVI, 1986* (Elsevier, Amsterdam, 1987), chap. 2.
24 H. J. M. Hanley, G. P. Morriss, T. R. Welberry and D. J. Evans, *Physica A*, 1988, **149**, 406.
25 D. C. Rapaport, *Phys. Rev. A*, 1987, **36**, 3288.

Paper 9/03069G; *Received* 19*th July*, 1989